Supporting Information (SI) *for*:

3D Self-assembled VS_4 Microspheres with High Pseudocapacitance as Highly Efficient anodes for Na-ion Batteries

*Wenbin Li,[a] Jianfeng Huang,[*a] Liangliang Feng,[*a] Liyun Cao,[a] Shuwei He, [a]*

[a] School of Materials Science & Engineering, Shaanxi University of Science and Technology, Xi'an Shaanxi 710021, P.R. China

E-mail: huangjf@sust.edu.cn; fengll@sust.edu.cn.

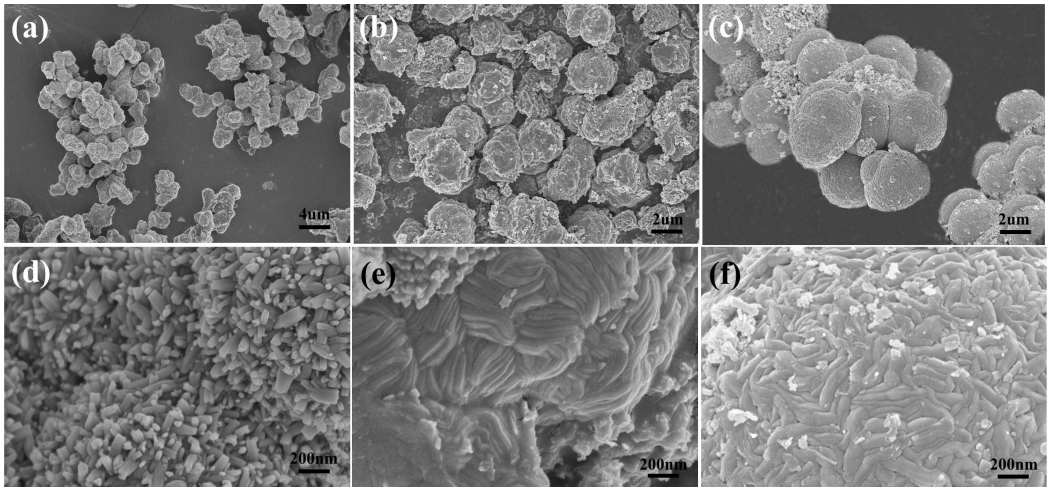

Fig. S1 SEM images of (a and d) VS_4-10, (b and e) VS_4-5 and (c and f) VS_4-3.

At lower pH value:

$$CH_3CSNH_2 + H_2O \rightarrow CH_3CONH_2 + H_2S\uparrow \quad \text{(S1)}$$

At higher pH value:

$$CH_3CSNH_2 + 2OH^- \rightarrow CH_3COO^- + HS^- + NH_3\uparrow \quad \text{(S2)}$$

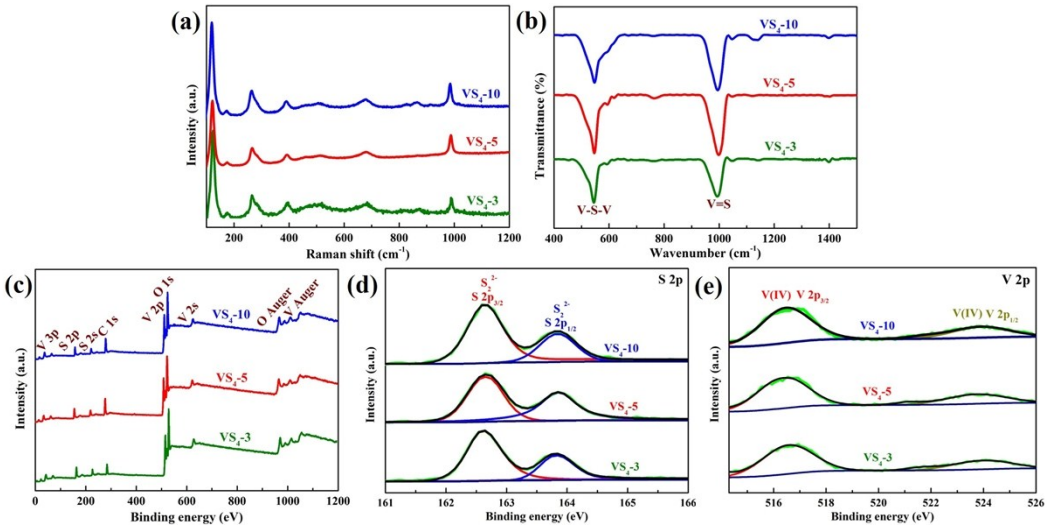

Fig. S2 (a) Raman spectra, (b) FTIR spectra, (c) Survey XPS spectra, High-resolution (d) S 2p and (e) V 2p XPS spectra of VS_4-10, VS_4-5 and VS_4-3.

As shown in Fig. S2(a), all Raman spectra appear almost identical with seven peaks located at 141, 191, 282, 406, 522, 689 and 992 cm^{-1}, which correspond to the bending and stretching vibrations of V-S bonds or their combination [1, 2]. When compared to their FTIR database in Fig. S2(b), three VS_4 products show two very similar peaks at 547 and 995 cm^{-1}, corresponding to the *v* (V-S-V) doubly bonded S^{2-} and the ν(V=S) terminal S stretches of VS_4, respectively [3, 4]. In addition, it can be clearly seen from the survey XPS spectra in Fig. S2(c) that all the samples have similar elemental composition, and their atomic ratios of V:S are close to 1:4. As displayed in Fig. S2(d and e), three VS_4 products exhibit very similar high-resolution S 2p XPS spectra with two S_2^{2-} 2p peaks at 162.7 and 163.9 eV, and V 2p XPS spectra with two V^{4+} 2p peaks at 516.5 and 523.8 eV [5, 6].

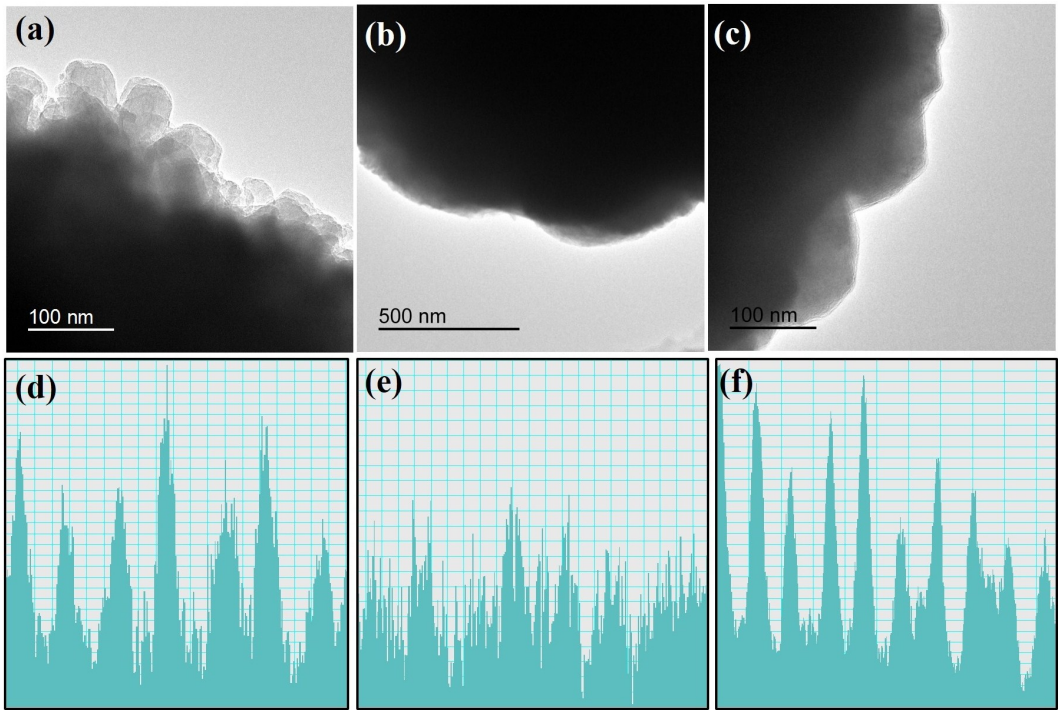

Fig. S3 High-magnification TEM images of (a) VS_4-10, (b) VS_4-5, (c) VS_4-3, and Histogram transform patterns of (d) VS_4-10, (e) VS_4-5, (f) VS_4-3 corresponding to HRTEM images in Fig. 4.

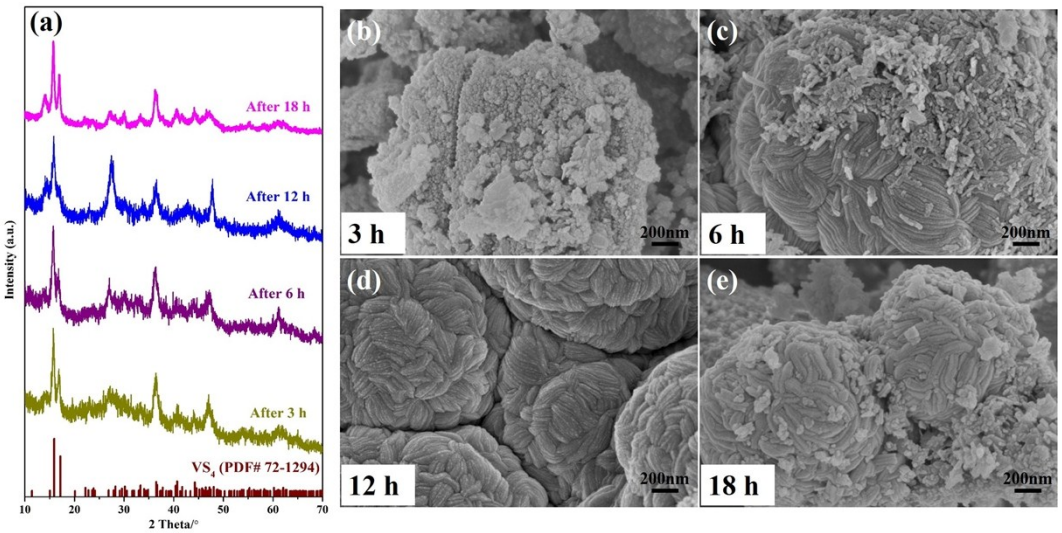

Fig. S4 (a) XRD patterns of the products collected after the hydrothermal reaction at pH=5 for different reaction times. SEM images of the products obtained at pH=5 for different reaction times: (b) 3 h, (c) 6 h, (d) 12 h and (e) 18 h.

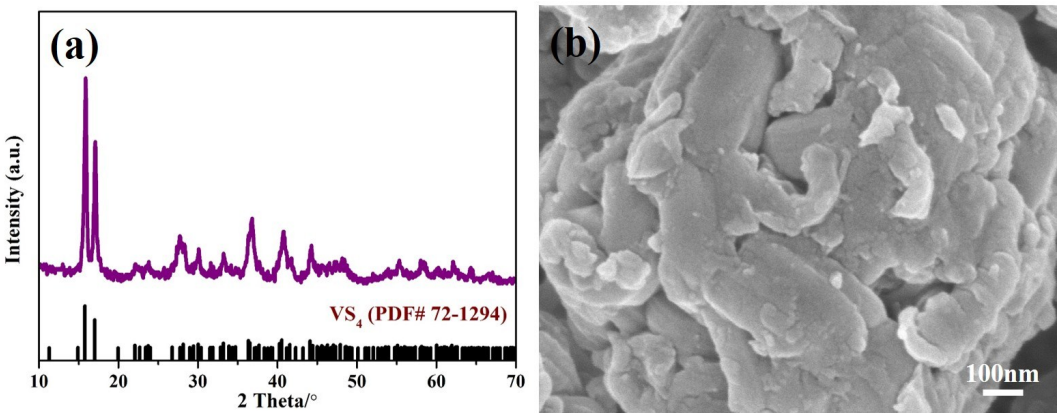

Fig. S5 (a) XRD pattern and (b) SEM image of the product obtained at pH=1 (1 g $NaVO_3$, 3.6 g C_2H_5NS, 180 ^oC, 24 h).

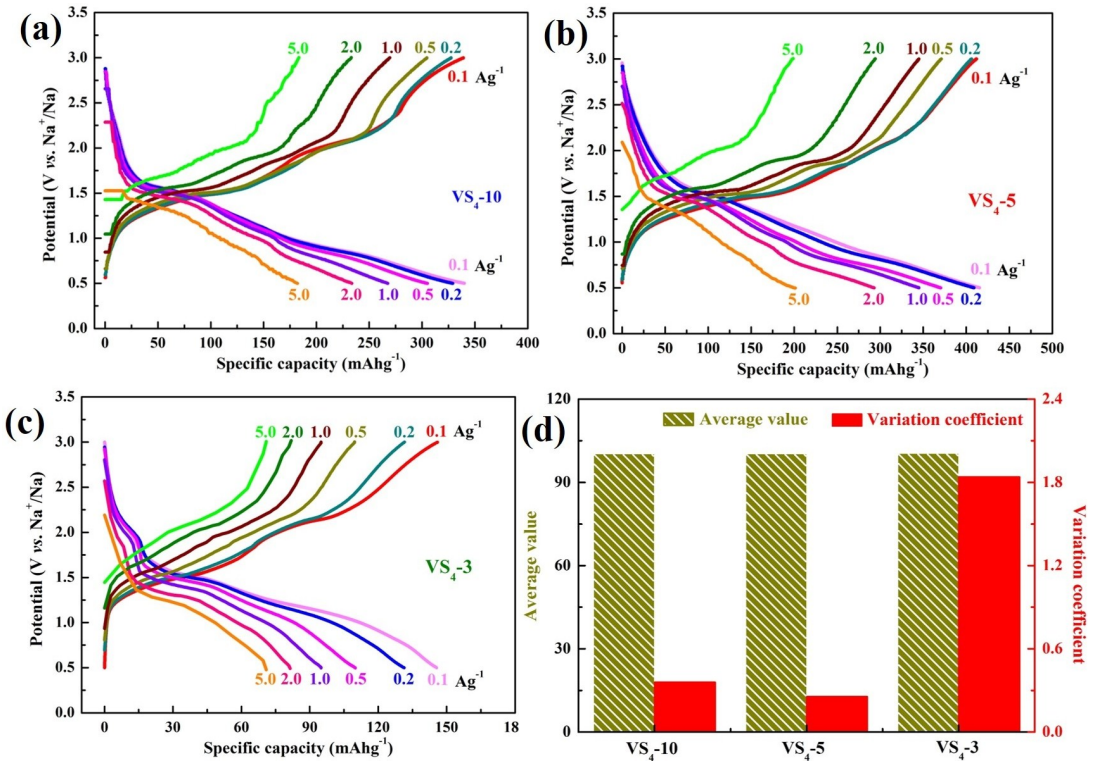

Fig. S6 Charge/discharge profiles of (a) VS_4-10, (b) VS_4-5 and (c) VS_4-3 electrode at various current densities from 0.1 to 5.0 Ag^{-1}. (d) Average values and variation coefficients of the CEs between the 70th and 300th cycle derived from Fig. 5(a).

Table S1 Electrochemical performance comparison of the as-prepared VS_4-5-based with other some V-based anode materials of SIBs.

Materials	Current density, Ag^{-1}	Cycling capacity, $mAhg^{-1}$, (cycle number, n)	Rate capacity, $mAhg^{-1}$, (Current density, Ag^{-1})	Cut-off voltage (V)	Active material loading, $mg \cdot cm^2$	Electrode composition	Ref
VS_4-5	**0.2**	**412(300)**	**408(0.2), 370(0.5), 345(1.0), 293(2.0), 201(5.0)**	**0.5~3.0**	**0.8 ~ 1.2**	**8:1:1**	**This work**
VS_4/rGO	0.5	149(100)	341(0.1), 267(0.3), 220(0.5), 192(0.8)	0.01~2.2	0.84~1.05	7:2:1	[1]
VS_4/GS	0.1	349.1(100)	314(0.1),299(0.2),277(0.5), 256(1.0), 234(2.0), 191(4.0)	0.3~3.0	~1.5	7:2:1	[7]
VS_2	0.2	245(100)	252(0.1), 211(0.5), 201(1.0), 196(2.0), 203(5.0)	0.4~2.2	0.84~1.05	7:2:1	[8]
ce-VS_2	1.0	109(100)	----	0.01~3.0	~1.0	7:2:1	[9]
VS_2@ $Na_2Ti_2O_5$	0.2	203(50)	233(0.1), 210(0.4), 161(1.0), 124(2.0), 75(4.0)	0.01~3.0	1.0~1.5	----	[10]
c-VS_2@VOOH	0.2	330(150)	424(0.1), 404(0.2), 356(0.5), 224(1.0), 140(2.0), 113(5.0)	0.5~3.0	0.6~1.0	8:1:1	[11]
VSe_2/C	0.1	467(50)	437(0.05), 375(0.1), 326(0.2), 309(0.5), 263(1.0), 132(2.0)	0~3.0	----	8:1:1	[12]

V_2O_5	0.04	177(100)	200(0.04), 185(0.08), 157(0.16), 130(0.32), 122(0.64)	1.0~4.0	~0.88mg	8:1:1	[13]
VO_2/rGO	0.4	123(200)	196(0.04), 178(0.08), 160(0.16), 134(0.4), 108(0.8)	0.25~3.0	----	8:1:1	[14]
FeV_2S_4	0.075	529(10)	548(0.075), 480(0.15), 372(0.375)	0~3.0	~3.0	8:1:1	[15]

The list of electrode composition ratio contains the active material, the conductive material and the binder.
----: The relevant data is not mentioned in the article.

Table S2 Charge/discharge plateau capacities and corresponding to plateau voltage ranges of VS_4-10, VS_4-5 and VS_4-3 electrode at the 180th cycle in Fig. 5(c).

Sample	VS_4-10	VS_4-5	VS_4-3
Discharge plateau capacity ($mAhg^{-1}$)	139	132	94
Voltage range (V)	1.101~1.613	1.083~1.620	1.095~1.630
Total discharge capacity	304	393	204
Charge plateau capacity ($mAhg^{-1}$)	151	166	88
Voltage range (V)	1.487~1.983	1.475~1.836	1.492~1.892
Total charge capacity	306	393	204

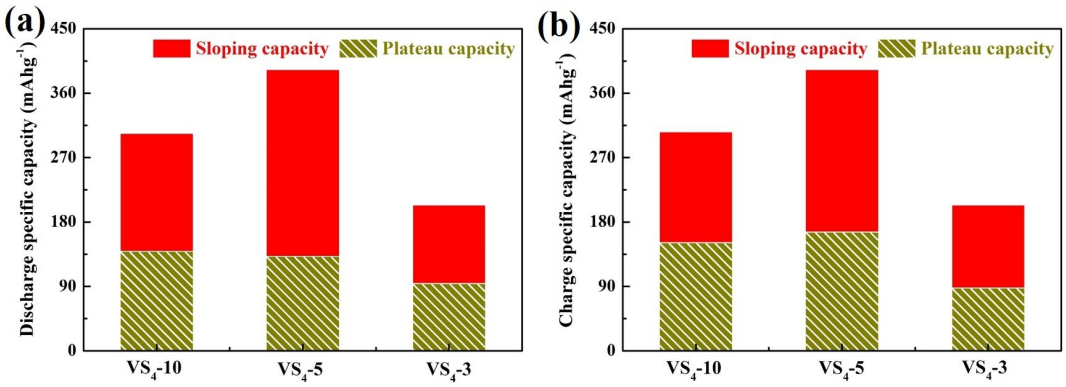

Fig. S7 Plateau capacities and sloping capacities of (a) discharge specific capacities and (b) charge specific capacities in Fig. 5(c) for VS_4-10, VS_4-5 and VS_4-3 electrode.

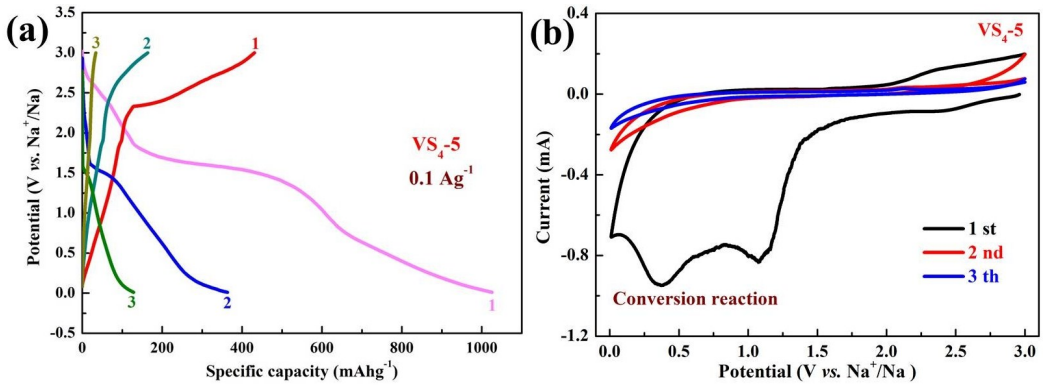

Fig. S8 (a) Charge/discharge profiles at 0.1 Ag^{-1} and (b) CV curves at a scan rate of 0.2 mVs^{-1} of VS_4-5 electrode.

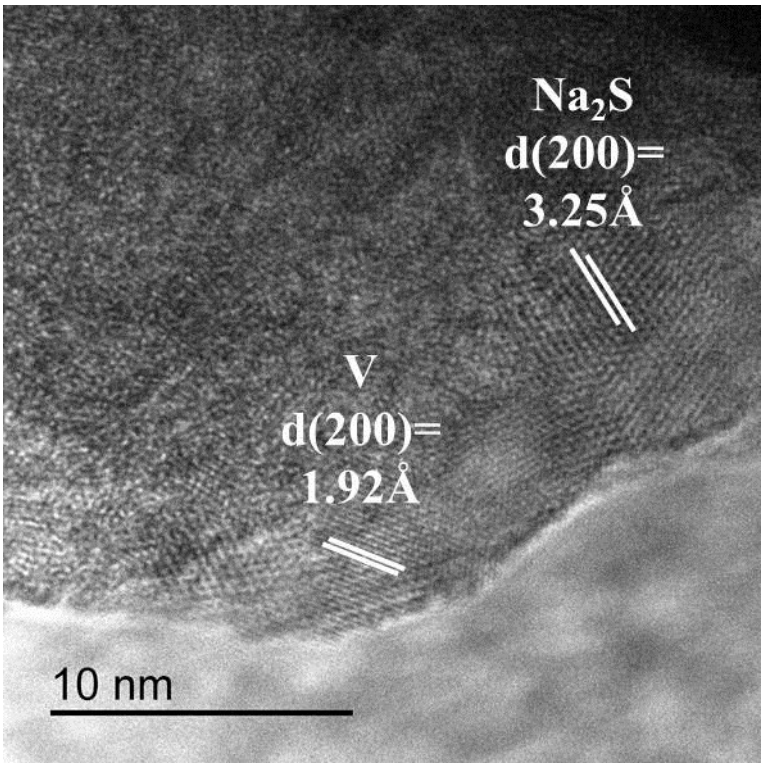

Fig. S9 HRTEM images of VS_4-5 electrode after discharged to 0.01 V at 0.02 Ag^{-1}.

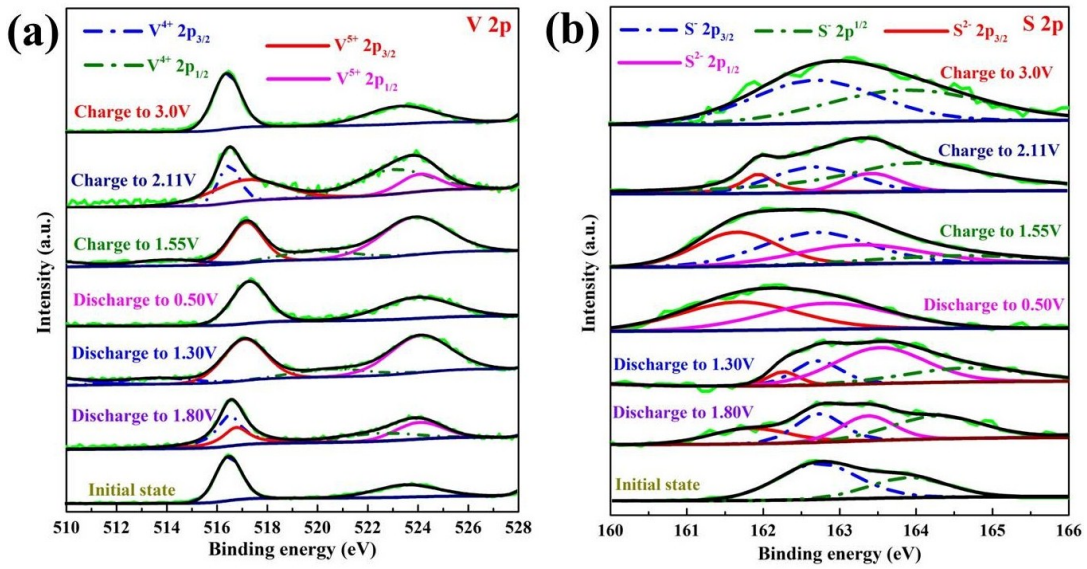

Fig. S10 High-resolution (a) V 2p and (b) S 2p XPS spectra of VS_4-5 electrode after discharging and charging to different potential states at 0.02 Ag^{-1}.

Table S3 Average valence of V and S, Number of Na^+ and corresponding Specific capacity for VS_4-5 electrode after discharging and charging to different potential states at 0.02 Ag^{-1}.

Potential state	Average valence of V	Average valence of S	Number of Na^+	Specific capacity ($mAhg^{-1}$)
Initial state	+4	-1	0	0
Discharge to 1.80V	+4.46	-1.36	0.98	243
Discharge to 1.30V	+4.80	-1.82	2.48	412
Discharge to 0.50V	+5	-2	3	675
Charge to 1.55V	+4.78	-1.52	1.3	-
Charge to 2.11V	+4.46	-1.19	0.3	-
Charge to 3.0V	+4	-1	0	-

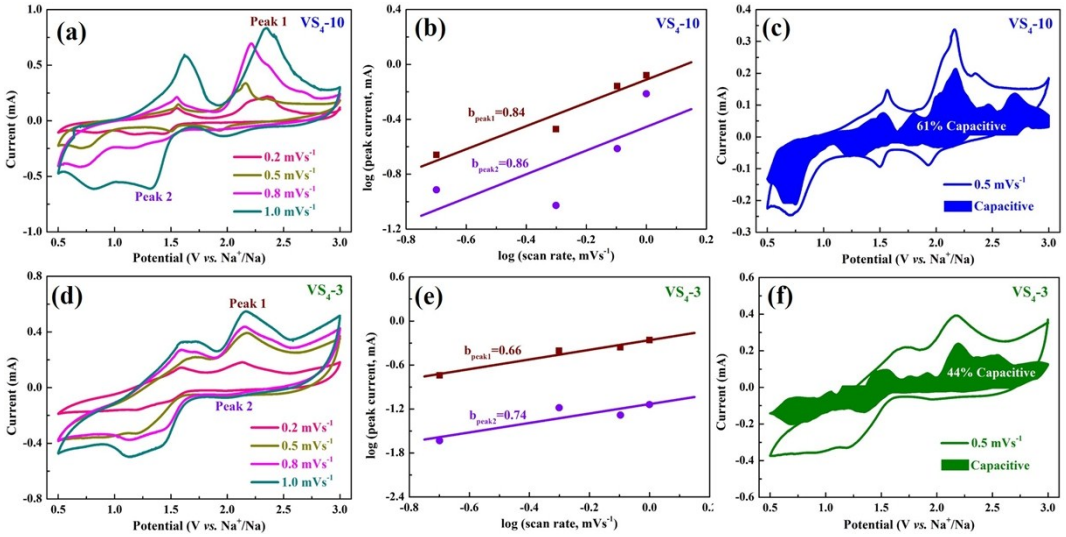

Fig. S11 CV curves of (a) VS_4-10 and (d) VS_4-3 electrode at different scan rates from 0.2 to 1.0 mVs^{-1}, The fitted lines and log (peak current) *vs*. log (scan rate) plots of (b) VS_4-10 and (e) VS_4-3 electrode at different oxidation and reduction states, and The capacitive contribution shown by the shaded region at 0.5 mVs^{-1} for (c) VS_4-10 and (f) VS_4-3 electrode.

$$\log(I) = b\log(\upsilon) + \log(a) \tag{S3}$$

$$I(\mathrm{V}) = k_{\mathrm{c}}\upsilon + k_{\mathrm{d}}\upsilon^{1/2} \tag{S4}$$

where a and b are adjustable parameters, I is the current (mA) and υ is the scan rate (mVs^{-1}). The b-value is determined by the slop of $\log(\upsilon)$ - $\log(i)$ plots. When b-value approaches to 0.5, the system is mainly controlled by a diffusion process, while b-value is closed to 1.0, the system is mainly controlled by a capacitive process [16]. The total current response ($I(\mathrm{V})$) at a fixed potential (V) can be divided into two parts including capacitive $I_{\mathrm{c}}(k_{\mathrm{c}}\upsilon)$ and diffusion-controlled $I_{\mathrm{d}}(k_{\mathrm{d}}\upsilon^{1/2})$ [17, 18]. The capacitive $I_{\mathrm{c}}(k_{\mathrm{c}}\upsilon)$ is composed of the faradaic contribution from the charge-transfer process occurring on the surface of electrode materials, referred to as pseudocapacitance; and the nonfaradaic contribution from double layer capacitive effect.

$$I_{(i)}(\mathrm{V}) = k_{\mathrm{c}}(\mathrm{V})\upsilon_i + k_{\mathrm{d}}(\mathrm{V})\upsilon_i^{1/2} \qquad i = 0.2, 0.5, 0.8, 1.0\ \mathrm{mVs^{-1}}; \tag{S5}$$

$$I_{(j)}(\mathrm{V}) = k_{\mathrm{c}}(\mathrm{V})\upsilon_j + k_{\mathrm{d}}(\mathrm{V})\upsilon_j^{1/2} \qquad j = 0.2, 0.5, 0.8, 1.0\ \mathrm{mVs^{-1}};\ i \neq j \tag{S6}$$

$$k_{\mathrm{c}(i\text{-}j)}(\mathrm{V}) = \left(\frac{I_{(j)}(\mathrm{V})}{\upsilon_j^{1/2}} - \frac{I_{(i)}(\mathrm{V})}{\upsilon_i^{1/2}}\right) \Big/ \left(\upsilon_j^{1/2} - \upsilon_i^{1/2}\right) \tag{S7}$$

$$k_{\mathrm{d}(i\text{-}j)}(\mathrm{V}) = \left(\frac{I_{(j)}(\mathrm{V})}{\upsilon_j} - \frac{I_{(i)}(\mathrm{V})}{\upsilon_i}\right) \Big/ \left(\upsilon_j^{-1/2} - \upsilon_i^{-1/2}\right) \tag{S8}$$

$$k_{\mathrm{c}}(\mathrm{V}) = \left(k_{\mathrm{c}(0.2\text{-}0.5)}(\mathrm{V}) + k_{\mathrm{c}(0.2\text{-}0.8)}(\mathrm{V}) + k_{\mathrm{c}(0.2\text{-}1.0)}(\mathrm{V}) + k_{\mathrm{c}(0.5\text{-}0.8)}(\mathrm{V}) + k_{\mathrm{c}(0.5\text{-}1.0)}(\mathrm{V}) + k_{\mathrm{c}(0.8\text{-}1.0)}(\mathrm{V})\right) \Big/ 6 \tag{S9}$$

$$k_{\mathrm{d}}(\mathrm{V}) = \left(k_{\mathrm{d}(0.2\text{-}0.5)}(\mathrm{V}) + k_{\mathrm{d}(0.2\text{-}0.8)}(\mathrm{V}) + k_{\mathrm{d}(0.2\text{-}1.0)}(\mathrm{V}) + k_{\mathrm{d}(0.5\text{-}0.8)}(\mathrm{V}) + k_{\mathrm{d}(0.5\text{-}1.0)}(\mathrm{V}) + k_{\mathrm{d}(0.8\text{-}1.0)}(\mathrm{V})\right) \Big/ 6 \tag{S10}$$

$$I_{\mathrm{c}(0.5)}(\mathrm{V}) = \frac{k_{\mathrm{c}}(\mathrm{V})}{k_{\mathrm{c}}(\mathrm{V}) + k_{\mathrm{d}}(\mathrm{V}) * 0.5^{-0.5}} I_{(0.5)}(\mathrm{V}) \tag{S11}$$

where $I_{(i)}(\mathrm{V})$ is the total current response at a fixed potential (V) and a fixed scan rate (i). $I_{(j)}(\mathrm{V})$ is the total current response at a fixed potential (V) and a fixed scan rate (j). υ_i and υ_j are the scan rate. $I_{\mathrm{c}(0.5)}(\mathrm{V})$ is the capacitive current response at a fixed potential (V) and a fixed scan rate of 0.5 $\mathrm{mVs^{-1}}$. $I_{(0.5)}(\mathrm{V})$ is the total current response at a fixed potential (V) and a fixed scan rate of 0.5 $\mathrm{mVs^{-1}}$.

Table S4 Resistance values simulated from modeling the experimental impedance (Fig. 8(a)) using the equivalent circuit shown in the insets in the bottom right of Fig. 8(a).

Samples	R_s (Ω)	$R_f + R_{ct}$ (Ω)	Θ(°)
VS_4-10	49.8	53.4	70.5
VS_4-5	30.5	12.5	76.8
VS_4-3	48.8	156.6	43.5

R_s is the electrolyte resistance. R_f is the SEI film resistance. R_{ct} is the charge-transfer resistance from electrolyte to active materials. Θ is the angle of the straight line at low frequency.

$$T_{sc} = (t_c + t_d)/(Q_c + Q_d) \quad \text{(S12)}$$

where T_{sc} is the charge/discharge time per unit specific capacity. t_c, t_d, Q_c and Q_d are the charge time, discharge time, charge specific capacity and discharge specific capacity at a fixed cycle.

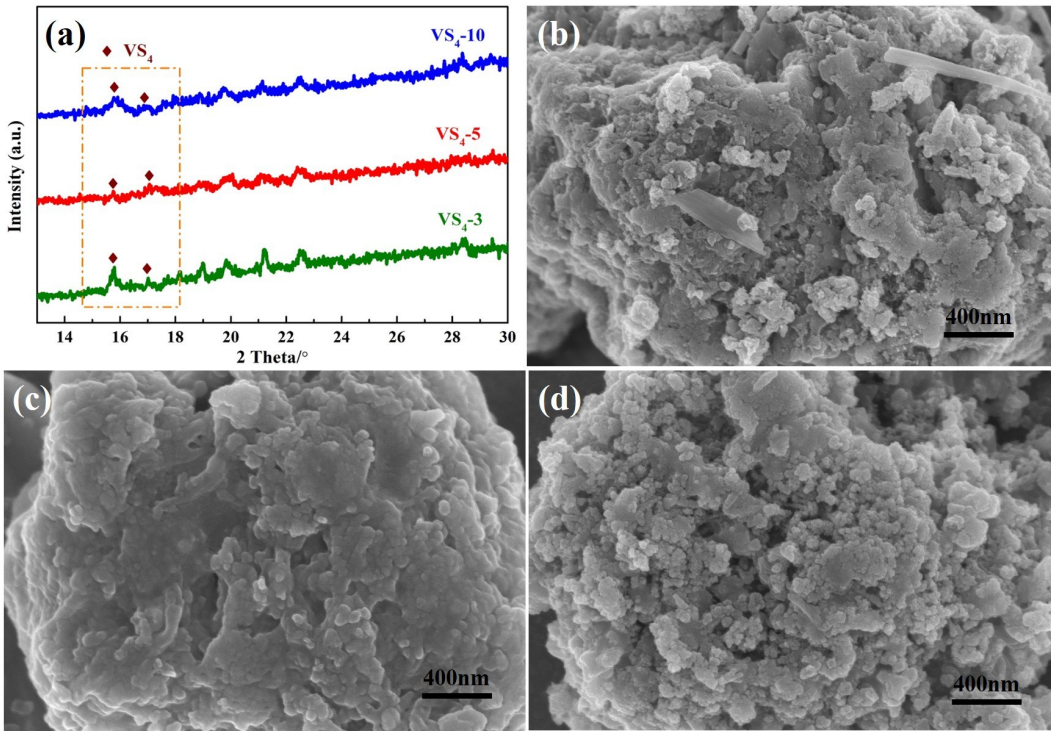

Fig. S12 (a) XRD patterns and SEM images of (b) VS_4-10, (c) VS_4-5 and (d) VS_4-3 after the rate and cycling tests.

References

1. R. Sun, Q. Wei, Q. Li, W. Luo, Q. An, J. Sheng, D. Wang, W. Chen and L. Mai, *ACS Appl. Mater. Interfaces*, 2015, **7**, 20902-20908.

2. M. N. Kozlova, Y. V. Mironov, E. D. Grayfer, A. I. Smolentsev, V. I. Zaikovskii, N. A. Nebogatikova, T. Y. Podlipskaya and V. E. Fedorov, *Chem.-Eur. J.*, 2015, **21**, 4639-4645.

3. Y. Zhou, Y. Li, J. Yang, J. Tian, H. Xu, J. Yang and W. Fan, *ACS Appl. Mater. Interfaces*, 2016, **29**, 18797-18805.

4. G. Lui, G. Jiang, A. Duan, J. Broughton, J. Zhang, M. W. Fowler and A. Yu, *Eng. Chem. Res.*, 2015, **54**, 2682-2689.

5. H. Liang, H. Shi, D. Zhang, F. Ming, R. Wang, J. Zhuo and Z. Wang, *Chem. Mater.*, 2016, **28**, 5587-5591.

6. C. S. Rout, B.-H. Kim, X. Xu, J. Yang, H. Y. Jeong, D. Odkhuu, N. Park, J. Cho and H. S. Shin, *J. Am. Chem. Soc.*, 2013, **135**, 8720-8725.

7. Q. Pang, Y. Zhao, Y. Yu, X. Bian, X. Wang, Y. Wei, Y. Gao and G. Chen, *ChemSusChem*, 2018, **11**, 735-742.

8. R. Sun, Q. Wei, J. Sheng, C. Shi, Q. An, S. Liu and L. Mai, *Nano Energy*, 2017, **35**, 396-404.

9. C. Yang, X. Ou, X. Xiong, F. Zheng, R. Hu, Y. Chen, M. Liua and K. Huang, *Energy Environ. Sci.*, 2017, **10**, 107-113.

10. J.-Y. Liao and A. Manthiramn, *Nano Energy*, 2015, **18**, 20-27.

11. W. Li, J. Huang, L. Feng, L. Cao, Y. Feng, H. Wang, J. Li and C. Yao, *J. Mater.*

Chem. A, 2017, DOI: 10.1039/c7ta05205g.

12. X. Yang and Z. Zhang, *Mater. Lett.*, 2017, **189**, 152-155.

13. D. Su, S. Dou and G. Wang, *ChemSusChem*, 2015, **8**, 2877-2882.

14. G. He, L. Li and A. Manthiram, *J. Mater. Chem. A*, 2015, **3**, 14750-14758.

15. M. Krengel, P. Adelhelm, F. Kleinc and W. Bensch, *Chem. Commun.*, 2015, **70**, 13500-13503.

16. Z. Hu, Z. Zhu, F. Cheng, K. Zhang, J. Wang, C. Chen and J. Chen, *Energy Environ. Sci.*, 2015, **8**, 1309-1316.

17. J. Wang, J. Polleux, J. Lim and B. Dunn, *J. phys. chem. c*, 2007, **111**, 14925-14931.

18. P. Simon, Y. Gogotsi and B. Dunn, *Science*, 2014, **343**, 1210-1211.